Structure and Dynamics of the Flexible Triple Helix of Water inside VPI-5 Molecular Sieves

Ettore Fois,* Aldo Gamba, and Antonio Tilocca

Dipartimento di Scienze Chimiche Fisiche e Matematiche, Universita' dell'Insubria at Como, Via Lucini 3, I-22100 Como, Italy

Received: November 20, 2001; In Final Form: February 13, 2002

The complex structural pattern described by water molecules in the channels of the large-pore VPI-5 aluminophosphate has been investigated through Car-Parrinello ab initio molecular dynamics simulations. Water molecules occupy crystallographic positions but considerably rotate and oscillate around their equilibrium positions. The extended network of strong hydrogen bonds among water in the channels leads to nonnegligible collective motions. The conformation of the triple helix formed by water molecules has been thoroughly examined; the helices run close to the channel walls and avoid the channel center. The high thermal motion of the water molecules makes such chains rather flexible and the helices are not easily detectable during the dynamics, but their shape emerges only when the average atomic positions are considered.

1. Introduction

In the last years there has been considerable interest in the behavior of water molecules adsorbed in the aluminophosphate molecular sieves.[1−5] VPI-5 is a crystalline large-pore aluminophosphate containing non-interconnected unidimensional channels made by 18-membered rings with diameter of $\approx$ 12 Å. Several interesting features of the water−VPI-5 system have been reported and are worth noting. First of all, the water arrangement in VPI-5 is ordered and reflects the symmetry of the lattice. According to the structural refinement of McCusker et al.[6] seven different water sites are present. Two water molecules are bound to the framework completing an octahedral coordination sphere about an aluminum atom; four of the remaining five form a triple helix of hydrogen-bonded molecules directed along the channel axis. The last kind of molecules, located near the center of the channel, link the helices to one another. The octahedral coordination at the aluminum site as well as the presence of two qualitatively different types of water (bound to aluminum and free) have been confirmed in several experimental studies.[1,3,12,13] However, the complex structure and the dynamical properties of the hydrogen-bonded chains have not been thoroughly investigated so far, apart from two NMR studies[1,3] where the interchange between free and bound molecules was examined. The behavior of water in zeolites with one-dimensional channels is an important topic in order to understand how specific guest−host and guest−guest interactions can determine the properties of sorbed molecules. In previous simulations[14−17] the differences in the behavior of water in zeolites characterized by small-diameter one-dimensional noncrossing channels have been highlighted. The zeolites considered there (namely, bikitaite, Li-ABW, and Na-ABW) have a high Al:Si ratio and small (8-ring) pores. Considerable differences emerged, mainly determined from the different composition (cation types and content) and framework structure. In this paper the properties of water in VPI-5 are studied through first-principles molecular dynamics (MD) simulations. It is interesting to compare the behavior of water molecules sorbed in this neutral, large-pore framework with those of the above-mentioned zeolites, which contain charge-balancing cations and possess much smaller pores. Apart from the general interest concerning confined water pointed out above, the present work is also aimed at providing a clear description of the chainlike structure of water molecules inside the VPI-5 cavities, as well as of their dynamical and structural properties.

2. Calculations

The chemical composition of the unit cell of VPI-5 is $[Al_{18}P_{18}O_{72}]\cdot 42H_2O$. The structure is shown in Figure 1. Following the X-ray Rietveld refinement of McCusker et al.,[6] we represented it in the $P6_3$ space group, with cell parameters $a = 18.9752$ Å and $c = 8.1044$ Å. The initial positions of water oxygens have been taken from the paper of McCusker et al., while the hydrogens have been initially placed in such a way to follow roughly the hydrogen-bond orientation of the chains proposed in the paper.[6] The dynamics of this system was simulated through the Car-Parrinello (ab initio) Molecular Dynamics method,[18,19] which allows to obtain a very accurate description of the system trajectory at finite temperature without the limitations implicit in the use of empirical potentials. The number of atoms included in the simulation (234) is rather large, and large computer resources are required. For this reason the calculations have been carried out on a parallel CRAY-T3E supercomputer: a single MD step takes about 1 min with 64 processors. A total of 456 valence electron states are contained in the system; they have been expanded in plane waves (including only the Γ point of the Brillouin zone) up to a cutoff energy of 60 Ry. The MD time step and the fictitious electronic mass were 5 and 500 atomic units, respectively. Periodic boundary conditions were applied to the hexagonal cell (we used the experimental lattice parameters[6]), and no symmetry constraint was imposed on the 234 atoms in the simulation cell. Norm-conserving pseudopotentials[20−22] represented ion−electron interactions, with d-nonlocality for aluminum, phosphorus, and oxygen atoms and a local pseudopotential for hydrogen. Electron−electron interactions were calculated with gradient-corrected density functional approximation;[23] in particular the

* Corresponding author.

10.1021/jp014276k CCC: $22.00
Published on Web 04/10/2002

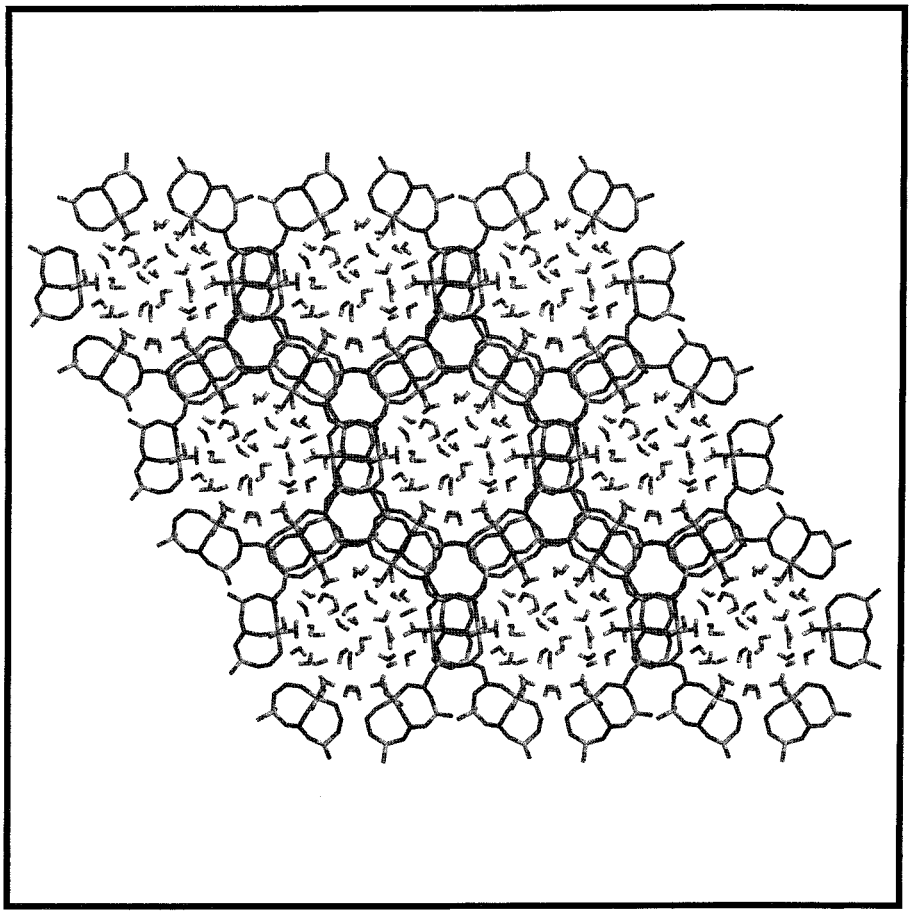

Figure 1. Structure of VPI-5 as seen along the *c* direction.

exchange functional of Becke[24] and the correlation functional of Perdew[25] were used. After an equilibration phase of 1.0 ps in which the system was thermalized at the temperature of 300 K by the Nosè thermostat,[26] the thermostat was turned off and a production run of about 50000 steps corresponding to a MD trajectory of 6.1 ps was carried out.

Empirical force fields-based MD simulations have been used for studying hydrated zeolites (see for example refs 7−10). The VPI-5 system itself has been simulated,[10] and a flexible effective potential for aluminophosphate lattices has recently been developed.[11] However, a fine-tuning of, for example, water-framework atoms potentials may be required for a meaningful simulation,[10] and an accurate knowledge of the system at the microscopic level may be needed.

The use of computationally costly first principles forces in atomistic trajectories implies that obtained results are unbiased by any parametrization procedure typical of empirical force fields, thus enhancing transferability and making comparison among different chemical and physical environments and with experiments more significant. Conventional MD could be useful to extend the simulations time scales; however, in the elapsed time of the present study rotational, vibrational, and thermal motions resulted sufficiently well sampled due to the crystallinity of the system.

3. Results and Discussion

The crystallographic atomic coordinates reported in Table 1 were calculated by folding each Cartesian coordinate to the asymmetric unit through the inverse symmetry operations of the $P6_3$ space group and then averaging them over the trajectory (atoms' labeling along the text, tables, and figures follows ref 6). The calculated values are plotted vs the experimental crystallographic coordinates[6] in Figure 2, and are reported in Table 1. The agreement is very good: only the *z* coordinate of

TABLE 1: Calculated and Experimental Fractional Crystallographic Coordinates for VPI-5[a]

atom	*x* (calc)	*x* (exp)	*y* (calc)	*y* (exp)	*z* (calc)	*z* (exp)	B_{iso} (calc)	B_{iso} (exp)
Al (1)	0.387	0.385	0.004	−0.001	0.242	0.239	0.653	0.24
Al (2)	0.470	0.474	−0.172	−0.173	0.195	0.204	0.596	0.24
Al (3)	0.653	0.654	0.173	0.169	0.200	0.198	0.683	0.24
P (1)	0.550	0.550	−0.001	−0.001	0.359	0.358	0.485	0.79
P (2)	0.309	0.311	−0.186	−0.185	0.317	0.320	0.624	0.79
P (3)	0.512	0.507	0.188	0.185	0.314	0.309	0.634	0.79
O (1)	0.473	0.470	0.002	0.001	0.356	0.339	1.578	1.5
O (2)	0.430	0.431	0.017	0.009	0.029	0.037	1.807	1.5
O (3)	0.325	0.322	−0.111	−0.112	0.223	0.223	1.341	1.5
O (4)	0.430	0.430	0.118	0.111	0.271	0.255	1.266	1.5
O (5)	0.543	0.540	−0.070	−0.074	0.243	0.264	1.412	1.5
O (6)	0.622	0.619	0.076	0.072	0.286	0.278	1.458	1.5
O (7)	0.518	0.512	−0.226	−0.231	0.261	0.280	1.340	1.5
O (8)	0.373	0.378	−0.211	−0.206	0.288	0.280	1.778	1.5
O (9)	0.455	0.474	−0.178	−0.175	−0.020	−0.015	1.300	1.5
O (10)	0.303	0.311	−0.175	−0.168	0.503	0.500	1.370	1.5
O (11)	0.576	0.575	0.201	0.195	0.183	0.198	1.361	1.5
O (12)	0.735	0.739	0.241	0.236	0.327	0.315	1.432	1.5
O_w (I)	0.336	0.339	−0.005	0.005	0.471	0.465	1.608	2.13
O_w (II)	0.287	0.290	0.002	0.002	0.151	0.160	1.874	2.13
O_w (III)	0.278	0.314	0.152	0.130	−0.032	−0.028	10.825	7.11
O_w (IV)	0.235	0.248	0.043	0.055	−0.243	−0.288	9.387	10.03
O_w (V)	0.197	0.193	0.060	0.045	−0.710	−0.566	12.65	10.03
O_w (VI)	0.323	0.319	0.192	0.189	−0.554	−0.539	7.560	7.11
O_w (VII)	0.111	0.100	0.060	0.053	−0.567	−0.534	16.332	10.03

[a] Atom labeling as in ref 6. O_w are water's oxygens. The last two columns report the isotropic temperature factors (Å^2).

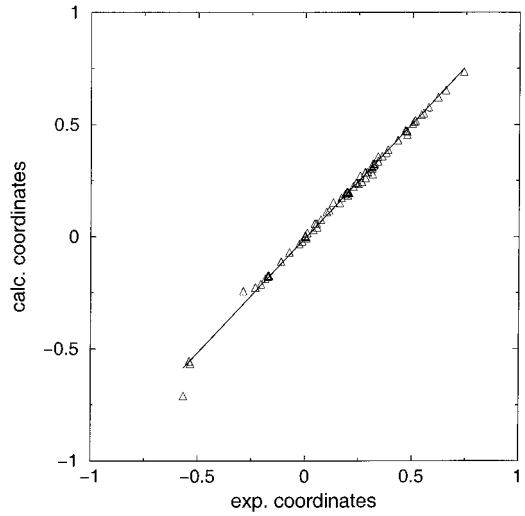

Figure 2. Calculated vs experimental fractional coordinates; the straight line is a linear fit.

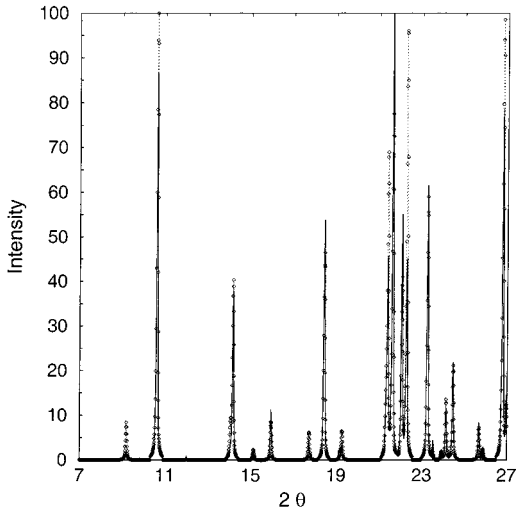

Figure 3. Simulated (continuous line) and experimental (dashed line with small circles) X-ray powder patterns.

TABLE 2: Average Closest Distances between Water Molecules Calculated as: (a) $\langle R_i \rangle - \langle R_j \rangle$; (b) $\langle \mathbf{R}_i - \mathbf{R}_j \rangle$ (labeling as in ref 6)

contact	(a) exp.	(a) sim.	(b)
I−II	2.63	2.78	2.79
II−V	3.24	2.69	2.91
II−VI	2.78	2.81	2.75
III−IV	2.50	2.49	2.79
IV−V	2.45	3.38	2.78
V−VI	2.59	2.75	2.87
V−VII	1.87	2.01	2.81
VI−VII	3.63	3.52	2.75
VII−VII	2.85	3.16	2.84

the H_2O (V) falls outside the straight line of unit slope. Therefore the experimental crystal structure is well reproduced in our simulation so that it is plausible that the same reliability also applies to the other calculated structural and dynamical properties. Looking in more detail at the distributions of the folded coordinates (not shown), it appears that those of the framework atoms (Al, P, and O) are in all cases rather narrow and centered on the experimental values. The same applies to the O atoms of the water molecules coordinated to Al, that is H_2O (I) and (II). The time needed for an interchange between these molecules and the free water[1] is much longer (of the order of milliseconds) than the simulation time, and we did not observe any such phenomenon: the octahedral coordination spheres remain unchanged for the whole trajectory. On the other hand, the distributions of the "free" water oxygens are broader, indicating a larger thermal motion about the crystal sites. Moreover, some of the distributions of the folded coordinates are centered on mean values different from the experimental ones. In almost all cases the averaging over such mean values (six for each coordinate) leads to coordinates very close to the experimental ones (Table 1 and Figure 2), with the only exception of the already mentioned *z* coordinate of the H_2O (V). However, when the *mean* folded coordinates are expanded again to build the unit cell and the closest distances between the water oxygens of three adjacent cells along *c* are calculated, some differences with the experimental distances are detected (Table 2). The largest differences (II−V and IV−V) involve the water (V), reflecting the displacement of the corresponding simulated $\langle z \rangle$ from the experimental value. A very short distance (2.01 Å) between H_2O (V) and (VII) is detected, which is rather unlikely and, indeed, never observed in the dynamics (look at the O−O radial distribution function reported below). Therefore the appearance of such short, fictitious distance is mainly related (as the trend of asymmetric unit coordinates discussed before) to the averaging made in the calculation of mean folded coordinates. Indeed, when the distances are calculated from the instantaneous positions during the trajectory (third column of Table 2) the V−VII separation results 2.81 Å. Anyway, due to the large thermal factors reported in Table 1, the "free" water molecules' positions show large fluctuations and their distances calculated from average coordinates are not very well-defined, so that the discrepancies in Table 2 should not be overemphasized. Moreover interatomic distances calculated from average positions are affected by errors because they do not take into account the correlation in the motion of the two atoms.[27] This correlation is correctly included only by the instantaneous interatomic distances averaged over time.

The simulated X-ray powder pattern has been calculated from the simulation data, namely the mean folded coordinates and the temperature factors U_{ij}, through the FOCUS program.[28] The U_{ij}'s matrix is calculated according to the following formula:

$$U_{ij}^{\mathrm{I}} = \frac{\int\int (x_i - X_i^{\mathrm{I}})(x_j - X_j^{\mathrm{I}}) D^{\mathrm{I}}(x_i, x_j)\, \mathrm{d}x_i\, \mathrm{d}x_j}{\int\int D^{\mathrm{I}}(x_i, x_j)\, \mathrm{d}x_i\, \mathrm{d}x_j} \qquad (1)$$

where i and $j = 1,2,3$, X^{I} are the average coordinates of atom I and $D^{\mathrm{I}}(x_i, x_j)$ is the pair distribution of the instantaneous positions x_i^{I} and x_j^{I}. Ensemble average is then performed over the trajectory. The isotropic temperature factors $B_{\mathrm{iso}} = 8\pi^2 U_{\mathrm{iso}}$ are reported in the Table 1. Figure 3 shows the simulated and experimental[6] X-ray powder diffraction patterns. The agreement is very good. Looking at the isotropic temperature factors it emerges that the bound water molecules are well localized in their coordination sites: their B_{iso} is similar to that of the framework oxygens. On the other hand the increase of almost 1 order of magnitude shown by the B_{iso} of the free molecules denotes a motion of considerably higher amplitude. The B_{iso}'s for the water hydrogens (not shown) confirm this point, ranging from ∼10 Å^2 for the bound molecules to 18−24 Å^2 for the free ones, i.e., about two times larger than the values for the corresponding oxygens. The direct inspection of the MD trajectory shows that the free waters do not diffuse but undertake large oscillations around the equilibrium positions. The largest temperature factor belongs to the H_2O (VII) molecules near the channel center, interestingly not directly involved in the triple

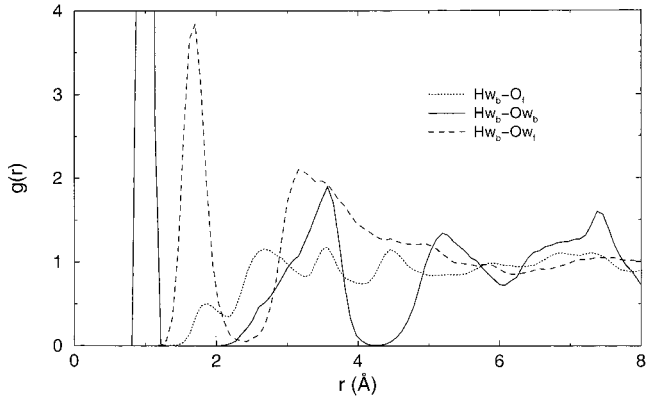

Figure 4. Bound water hydrogen−oxygen radial distribution functions.

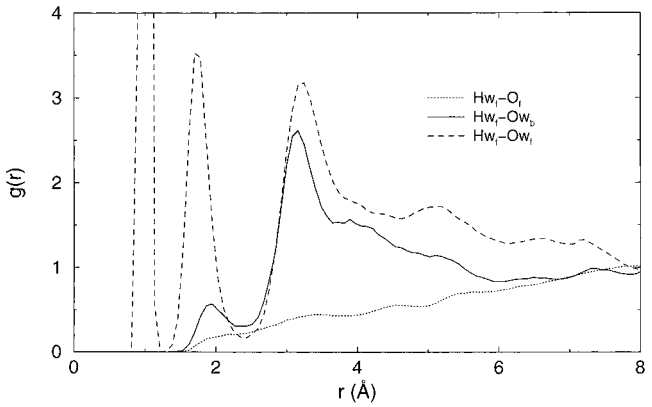

Figure 5. Free water hydrogen−oxygen radial distribution functions.

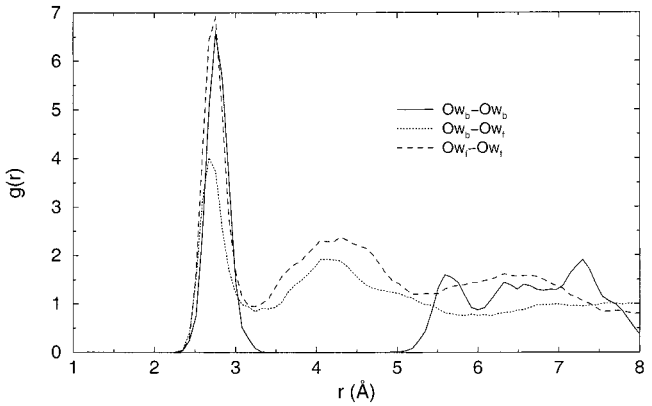

Figure 6. Oxygen−oxygen radial distribution functions for free and bound water.

helix. The H_2O (VI) turns out to be the least mobile among the free waters. The radial distribution functions (rdfs) have been calculated separately for the bound and free water. Figure 4 reports the bound water hydrogen−oxygen rdfs, while in Figure 5 the free water hydrogen−oxygen rdfs are shown. From Figure 4 it emerges that bound water forms strong hydrogen bonds with free water (with the bound water acting as H-donor) and interacts only weakly with framework oxygens; no hydrogen bonds are formed with the second coordinated water. The intense and sharp peak around 1.6 Å in Figure 5 highlights an extended network of strong hydrogen bonds between free water molecules. The free−bound interaction with the free water acting as hydrogen-bond donor is weaker than the reverse one, but not negligible. No significant interaction with the framework is detected. The water oxygen−water oxygen rdfs (Figure 6) show a peak at ∼2.8 Å for both free and bound molecules. However, as the hydrogen rdfs show that there is no hydrogen bond between the two bound waters, the peak for the bound water can be ascribed to their static arrangement in the octahedral coordination.

The conformation of the water chains then begins to be unveiled: the free waters form a network of hydrogen bonds, and one of the bound water molecule, H_2O (II), takes part in this network. It starts a chain by linking a free water. As we will show below, the chain is further propagated via free molecules till one more bound water is reached. The second bound water is linked to the aluminum atom in the next layer, rotated by 60° in the *xy*-plane and translated by *c*/2 with respect to the starting aluminum. The chain is continued following this pattern. Three such chains grow in this way along the channel, starting from aluminum atoms located at the same value of *z* and at 120° from each other. As in bikitaite and ABW zeolites,[16] the interaction of the water molecules with the framework oxygens is very weak. However, in VPI-5 there is a strong interaction between the bound water and framework aluminum. Water (I) and (II) are strongly "pinned" to the aluminum cations and favor the formation of helicoidal chains of free waters which connect the aluminum-bonded waters.

As can be inferred from the high thermal factors of free water, the dynamic behavior of the chains may be affected by the effective mobility of water molecules around their crystallographic sites. In addition to the temperature factors discussed above, further information concerning water's effective motion can be extracted from the Single Molecule Orientational Relaxation $\phi(t)$ (SMOR) and the Collective Orientational Relaxation (COR) $\Phi(t)$[29]

$$\phi(t) = \langle \mu(t)\cdot\mu(0)\rangle/\langle \mu^2\rangle \tag{2}$$

$$\Phi(t) = \langle \mathbf{M}(t)\cdot\mathbf{M}(0)\rangle/\langle M^2\rangle \tag{3}$$

where μ is the dipole moment vector of a single molecule and $\mathbf{M}$ is the total dipole of the molecules; μ has been approximated by the bisector of the HOH angle. The molecular rotation induces the decay of $\phi(t)$; when a molecule is involved in a number of hydrogen bonds, like in liquid water, the decay will be slower because a rotation involves the breaking of such bonds. On the other hand, if the molecule is frozen in its crystallographic site and does not rotate (as it occurs in bikitaite) only fast librations are possible, leading to a fast decay of $\phi(t)$. The short-time SMOR and COR curves for the zeolitic systems and liquid water (the latter taken from ref 30) are shown in Figure 7. In VPI-5, the relaxation of $\phi(t)$ is slightly slower than for the ABW systems, while it is considerably faster than for liquid water. This indicates that water in VPI-5 does rotate and the molecules have a greater rotational freedom than liquid water, where the rotation requires the breaking of about four hydrogen bonds, while a smaller number of hydrogen bonds per molecule is formed in VPI-5 (and in bikitaite and ABW zeolites). The comparison between COR and SMOR gives information about the collective effects related to the intermolecular interactions: when the rotation of a molecule involves a change of orientation with respect to neighboring molecules (requiring some energy to change the direction of dipoles), a slower relaxation of the total dipole will arise and the COR decay will be slower than the SMOR one because the first includes the collective motion through the cross-terms in the correlation function. When such collective effects are small, the SMOR and COR curves will coincide. Figure 7 shows that a small but nonnegligible collective interaction is present in VPI-5. In the lower right corner of Figure 7 the *y*-component of SMOR in VPI-5 is compared for free and bound water

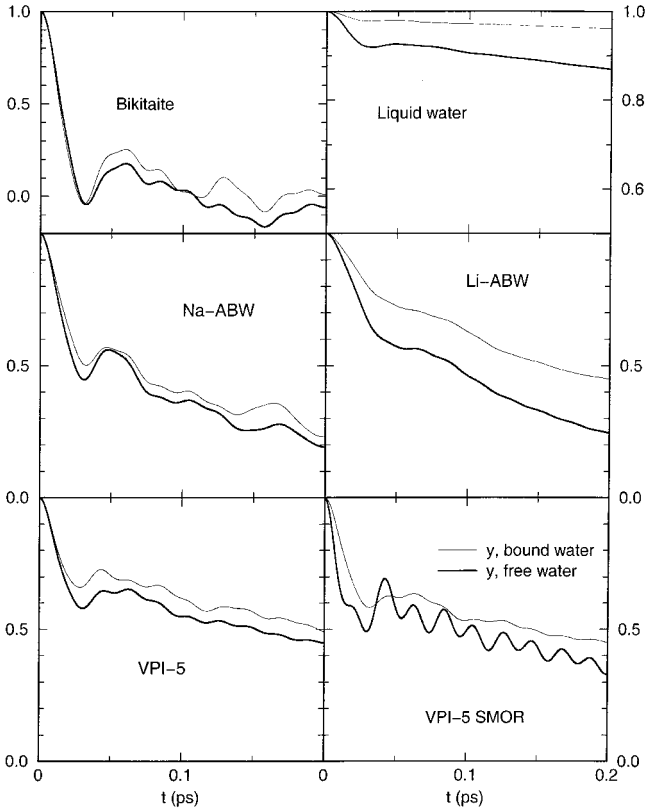

Figure 7. Collective Orientational Relaxation (thin lines) and Single-Molecule Orientational Relaxation (thick lines) curves. The bottom right figure shows the *y*-component of the SMOR for bound and free water.

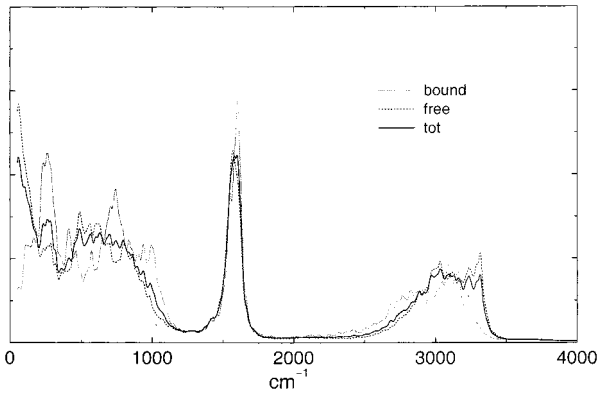

Figure 8. Total vibrational spectrum for water molecules and the contribution of bound and free molecules.

molecules. The free water appears to rotate more effectively than the bound molecules: this is rather surprising because each free water is usually involved in two (or more) hydrogen bonds, while the bound molecules form on average 0.5 hydrogen bonds per molecule: thus the chemisorption of the bound molecules to the framework strongly hinders their rotational motion.

Molecular vibrations are strongly affected by interactions, and a spectroscopic study could be a viable tool in unravelling the complex behavior of water in VPI-5. Unfortunately, to the best of our knowledge, no VPI-5 IR spectrum has been so far reported. The vibrational spectrum of water molecules can be calculated as Fourier transform of the velocity autocorrelation function. The total spectrum as well as the contribution of bound and free water molecules are reported in Figure 8. The stretching band of the total spectrum extends over a large region (about 900 cm^{-1}) and it appears to be slightly red-shifted with respect to the stretching band of liquid water calculated with the same

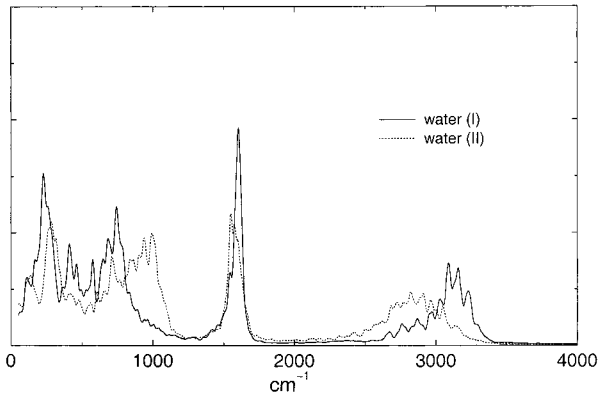

Figure 9. Vibrational spectrum of bound water (I) and (II).

method and energy functionals[31] (centered at 3200 cm^{-1}). This is to be ascribed both to the strong hydrogen bonds and to the interaction of the bound molecules with aluminum, which weaken the O−H intramolecular bonds. Indeed the stretching band of the bound molecules, involved both in hydrogen bonds with the free molecules and in the octahedral coordination sphere of aluminum is further red-shifted. The vibrational density below 1000 cm^{-1} arises both from the librational modes and from the coupling to the framework modes. A sharp peak near 700 cm^{-1} is present for the bound water. In Figure 9 the contributions of (I) and (II) bound water molecules to the vibrational spectrum are separated. The H_2O (II) are hydrogen bonded to free water molecules and also coordinated to aluminum, while the bound H_2O (I) do not form hydrogen bonds. This leads to a considerable red-shift of the stretching band for H_2O (II), which is centered at 2900 cm^{-1}, and also to a blue-shift of their librational band.

To visualize the conformation of the three helices the following method has been adopted: the average atomic coordinates of the unit cell were translated over six unit cells superimposed along *z*. Each of the three helices was built from these extended coordinates by starting from a H_2O (II) oxygen and finding the next oxygen hydrogen bonded to it (i.e., the O atom located at less than 2.9 Å from it); then the chain was continued starting from the last oxygen atom, and so on. If no molecules hydrogen bonded to the last atom were found, it was removed from the sequence: the search for neighbors was restarted from the previous oxygen in the chain, but now excluding the oxygen just removed. Figure 10 shows the structure of the three helices obtained in this way. Two main points emerge: the three chains grow and intersect each other along the channel walls, always avoiding the channel center where the H_2O (VII) are located. Each chain develops toward the *z* direction connecting octahedral Al atoms located at increasing height along the channel. Moreover, the chains resulted formed only by II, V, and VI water molecules: the sequence of water molecules in the chain is II−V−VI−II− ...; the III and IV molecules are close to each other, but their distance from the other water molecules is larger than 2.9 Å. This is a dynamical effect, because when the above method is applied to the crystallographic (experimental) coordinates, the "regular" II−III−IV−V−VI−II− ... sequence is found, whose shape is similar to the other one except for a small additional "loop" along the chain. Moreover the nonnegligible thermal fluctuations in the oxygens' positions are such that the instantaneous configuration of the chains is ill-defined: the method devised to visualize the chains works only when the average geometry is considered, but when it is applied to an instantaneous configuration the clear sequence described above does

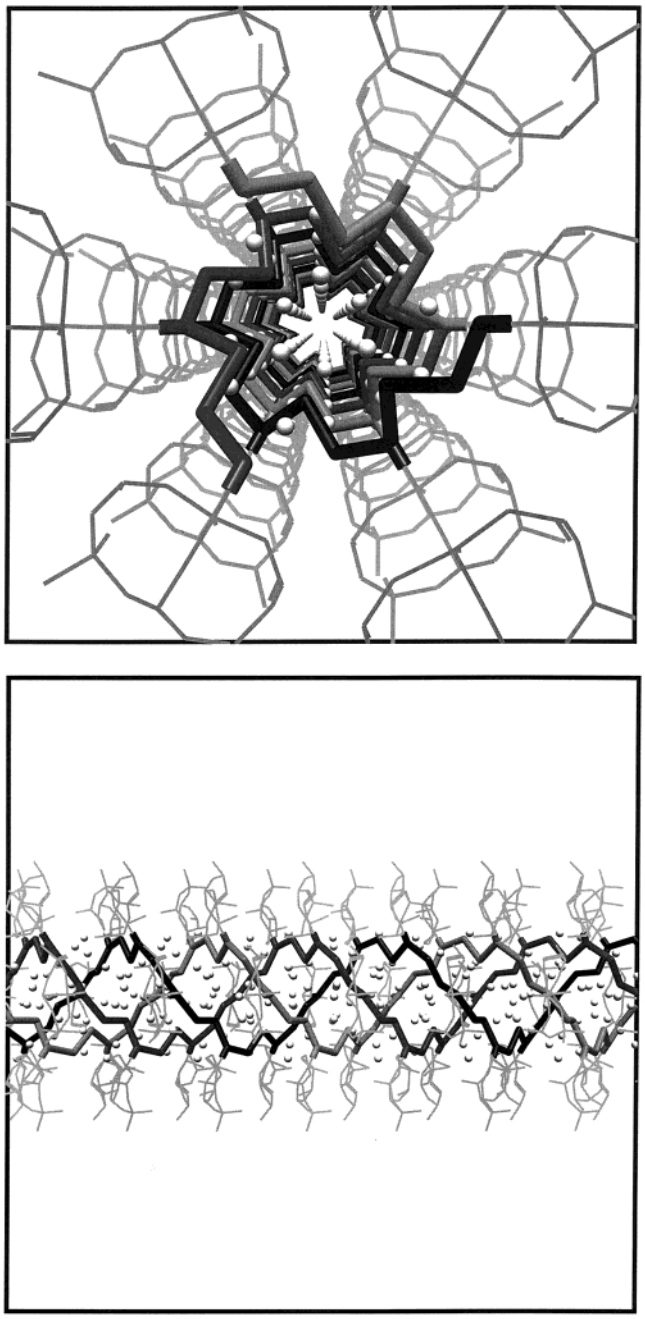

Figure 10. (a) Pictorial view of the conformation of the three helices along the channel, obtained by joining together the hydrogen-bonded water oxygens in each chain with lines of different color. The white spheres represent water oxygens not involved in the three helices. (b) The same representation as in (a), rotated by 90° along *x*.

not always emerge and a clear-cut definition of the three helices as in Figure 10 is no longer possible. At room temperature, due to the water's relevant thermal motion, the triple helix structure is therefore highly flexible. The large temperature factors, found in experiments and confirmed by our simulation, are an indication of large amplitude displacements from equilibrium positions which determine the instantaneous breaking of the chains in a number of positions.

Further information on the microscopic arrangement of water molecules inside the cavity has been obtained by looking at their distribution in the *xy*-plane normal to the channel axis.[32] The water molecules were divided into 10 concentric shells according to their distance from the center of the pore projected on such plane. The average density and number of hydrogen

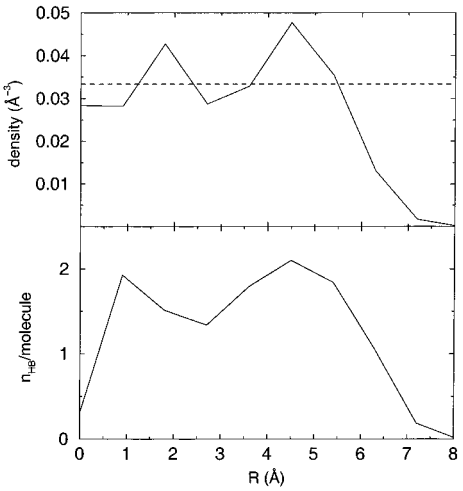

Figure 11. Top: Average density profile along the pore radius. The horizontal dashed line indicates the density of bulk liquid water. Bottom: Average number of hydrogen bonds per molecule, again as a function of the distance from the pore center.

bonds per molecule in each shell are shown in Figure 11. Two well-defined layers of water molecules, located at 1−2 Å and 4−5 Å from the center of the cavity, are evident: the latter corresponds to the water helices near the VPI-5 surface. In both layers each molecule is hydrogen bonded to no more than two neighboring molecules, while in the less dense intermediate region the number of hydrogen bonds is obviously reduced. This confirms that the greater freedom experienced by the molecules closest to the channel center is not sufficient to break the ordered arrangement and form a liquidlike bulk phase. This phenomenon has been observed for the inner layers of water molecules sorbed in the much larger pores of Vycor glass at full hydration.[32,33]

4. Conclusions

The intensive calculations presented in this paper allowed us to clarify some of the properties of water molecules sorbed in the large pores of neutral crystalline VPI-5 aluminophosphate. In particular, we think to have elucidated the characteristics of the helicoidal chains of water molecules from both a static and a dynamical point of view. The triple helix pattern extracted from the calculated mean crystallographic coordinates gathers the main features of the same structure obtained by McCusker et al.[6] on the basis of powder diffraction data. However, when the motion of the water molecules is directly taken into account, the large thermal motion of free water molecules involved in the chains often breaks up the water−water links within the chains and does not allow an equally clear picture to be obtained for each instantaneous configuration. The strong octahedral coordination of two water molecules to aluminum atoms determines several important effects: seemingly, it is the basic factor which drives the formation of chains; the strong interaction with aluminum determines deep differences in the behavior of the bound and the free molecules, evidenced by the thermal factors, the vibrational spectra, and the orientational correlation functions. The hydrogen-bond network, while being rather flexible, gives water a solidlike character not only in the layer of molecules near the surface, but also in the region close to the channel center. The diameter of the VPI-5 pores is still too small to allow the molecules close to the center to form a bulk liquid phase. The effect of the confinement and the interaction with the framework, albeit stronger for the molecules near the surface, is transmitted through hydrogen bonds from the walls to the channel center, where molecules show only a slightly

larger rotational and vibrational freedom. They however do not diffuse and their oxygen atoms, both from the simulation and X-ray data, result to have a defined crystalline structure.

References and Notes

(1) Goldfarb, D.; Li, H.; Davis, M. E. *J. Am. Chem. Soc.* **1992**, *114*, 3690.

(2) Kustanovich, I.; Goldfarb, D. *J. Phys. Chem.* **1991**, *95*, 1991.

(3) Duer, M. J.; He, H.; Kolodziejski, W.; Klinowski, J. *J. Phys. Chem.* **1994**, *98*, 1198.

(4) Prasad, S.; Vetrivel, R. *J. Phys. Chem.* **1994**, *98*, 1579.

(5) Kitao, O.; Gubbins, K. E. *J. Phys. Chem.* **1996**, *100*, 12424.

(6) McCusker, L. B.; Baerlocher, C.; Jahn, E.; Bülow, M. *Zeolites* **1991**, *11*, 308.

(7) Demontis, P.; Suffritti, G. B.; Alberti, A.; Quartieri, S.; Fois, E.; Gamba, A. *Gazz. Chim. Ital.* **1986**, *116*, 459.

(8) Cicu, P.; Demontis, P.; Spanu, S.; Suffritti, G. B.; Tilocca, A. *J. Chem. Phys.* **2000**, *112*, 8267.

(9) Leherte, L.; André, J.-M.; Derouane, E. G.; Vercauteren, D. P. *J. Chem. Soc., Faraday Trans.* **1991**, *87*, 1959.

(10) Trouw, F.; Iton, L. E.; Davis, M. E. *Stud. Surf. Sci. Catal.* **1994**, *84*, 854−858.

(11) Demontis, P.; Gulín González, J.; Suffritti, G. B.; Tilocca, A.; de las Pozas, C. *Microporous Mesoporous Mater.* **2001**, *42*, 103.

(12) Grobet, P. J.; Samoson, A.; Geerts, H.; Martens, J. A.; Jacobs, P. A. *J. Phys. Chem.* **1991**, *95*, 9620.

(13) Rocha, J.; Kolodziejski, W.; He, H.; Klinowski, J. *J. Am. Chem. Soc.* **1992**, *114*, 4884.

(14) Quartieri, S.; Sani, A.; Vezzalini, G.; Galli, E.; Fois, E.; Gamba, A.; Tabacchi, G. *Microporous Mesoporous Mater.* **1999**, *30*, 77.

(15) Fois, E.; Tabacchi, G.; Quartieri, S.; Vezzalini, G. *J. Chem. Phys.* **1999**, *111*, 355.

(16) Fois, E.; Gamba, A.; Tabacchi, G.; Quartieri, S.; Vezzalini, G. *J. Phys. Chem. B* **2001**, *105*, 3012.

(17) Fois, E.; Gamba, A.; Tabacchi, G.; Quartieri, S.; Vezzalini, G. *Phys. Chem. Chem. Phys.* **2001**, *3*, 4158.

(18) Car, R.; Parrinello, M. *Phys. Rev. Lett.* **1985**, *55*, 2471.

(19) Hutter, J.; Ballone, P.; Bernasconi, M.; Focher, P.; Fois, E.; Goedecker, S.; Parrinello, M.; Tuckerman, M. *CPMD code, version 3.0*; MPI für Festkörperforschung, Stuttgart, and IBM Zürich Research Laboratory, 1990−1996.

(20) Hamann, D.; Schlüter, M.; Chiang, C. *Phys. Rev. Lett.* **1979**, *43*, 1494.

(21) Kleinman, L.; Bylander, D. *Phys. Rev. Lett.* **1982**, *48*, 1425.

(22) Troullier, N.; Martins, J. *Phys. Rev. B* **1991**, *43*, 1993.

(23) Parr, R.; Yang, W. *Density Functional Theory of Atoms and Molecules*; Oxford University Press: Oxford, 1989.

(24) Becke, A. *Phys. Rev. A* **1988**, *38*, 3098.

(25) Perdew, J. *Phys. Rev. B* **1986**, *33*, 8822.

(26) Nosè, S. *Mol. Phys.* **1984**, *52*, 255.

(27) Willis, B. T. M.; Pryor, A. W. *Thermal Vibrations in Crystallography*; Cambridge University Press: London, U.K., 1975.

(28) Grosse-Kunstleve, R.; McCusker, L.; Baerlocher, C. *J. Appl. Crystallogr.* **1999**, *32*, 536.

(29) Ohmine, I. *J. Phys. Chem.* **1995**, *99*, 6767.

(30) Fois, E.; Gamba, A.; Redaelli, C. *J. Chem. Phys.* **1999**, *110*, 1025.

(31) Laasonen, K.; Sprik, M.; Parrinello, M. *J. Chem. Phys.* **1993**, *99*, 9080.

(32) Rovere, M.; Ricci, M. A.; Vellati, D.; Bruni, F. *J. Chem. Phys.* **1998**, *108*, 9859.

(33) Hartnig, C.; Witschel, W.; Spohr, E.; Gallo, P.; Ricci, M. A.; Rovere, M. *J. Mol. Liq.* **2000**, *85*, 127.